HHS Public Access

Author manuscript

*Acad Radiol*. Author manuscript; available in PMC 2018 May 01.

Published in final edited form as:

*Acad Radiol*. 2017 May ; 24(5): 594–602. doi:10.1016/j.acra.2016.12.007.

# Ventricular geometry from non-contrast non-ECG gated CT scans: an imaging marker of cardiopulmonary disease in smokers

**Farbod N. Rahaghi**[1,*], **Gonzalo Vegas Sánchez-Ferrero**[2,8,*], **Jasleen K. Minhas**[1], **Carolyn E. Come**[1], **Isaac De La Bruere**[1], **J. M. Wells**[3], **Germán González**[2], **Surya P. Bhatt**[3], **Brett E. Fenster**[5], **Alejandro A. Diaz**[1], **Puja Kohli**[6], **James C. Ross**[2], **David A. Lynch**[7], **Mark T. Dransfield**[3], **Russ P. Bowler**[4], **Maria J. Ledesma-Carbayo**[8], **Raúl San José Estépar**[2,++], **George R Washko**[1,++], and **the COPDGene Investigators**

[1]Brigham and Women's Hospital, Pulmonary and Critical Care Division of Department of Medicine 75, Francis Street, PBB – CA 3 Boston, MA 02115

[2]Department of Radiology, Harvard School of Medicine, University of Alabama at Birmingham

[3]Division of Pulmonary, Allergy and Critical Care Medicine, University of Alabama at Birmingham

[4]Division of Pulmonary, Critical Care and Sleep Medicine, Department of Medicine National Jewish Health, 1400 Jackson St. Denver, CO 80206

[5]Division Cardiology, Department of Medicine, National Jewish Health, 1400 Jackson St. Denver, CO 80206

[6]Massachusetts General Hospital, Pulmonary and Critical Care Division of Department of Medicine, 1400 Jackson St. Denver, CO 80206

[7]Department of Radiology, National Jewish Health, 1400 Jackson St. Denver, CO 80206

[8]Biomedical Image Technologies, Universidad Politécnica de Madrid & CIBER-BBN, Madrid, Spain

## Abstract

Correspondence to: Farbod N. Rahaghi.

[*]Equal contributors on this manuscript

[++]Equal contributors on this manuscript



Conception and design: GVSF, RSJE, FNR, GRW,CEC, DEL, RPB, PK;
Algorithmic development: GVSF, GGS, JCR, MJLC, RSJE;
Data Collection and analysis: FNR, GVSF, JKM, IDLB, JMW, SPB, BEF, DEL, MTD, RPB;
Statistical Analysis: FNR, CEC, AAD, GRW;
Manuscript preparation: FNR, GVSF, JKM, CEC, AAD, RSJE, GRW;

**Disclosures**
None

**Background—**Imaging based assessment of cardiovascular structure and function provides clinically relevant information in smokers. Non-cardiac gated thoracic computed tomographic (CT) scanning is increasingly leveraged for clinical care and lung cancer screening. We sought to determine if more comprehensive measures of ventricular geometry could be obtained from CT using an atlas based surface model of the heart.

**Methods—**Subcohorts of 24 subjects with cardiac MRI and 262 subjects with echocardiography were identified from COPDGene, a longitudinal observational study of smokers. A surface model of the heart was manually initialized, and then automatically optimized to fit the epicardium for each CT. Estimates of right and left ventricular (RV and LV) volume and free wall curvature were then calculated and compared with structural and functional metrics obtained from MRI and echocardiograms.

**Results—**CT measures of RV dimension and curvature correlated with similar measures obtained using MRI. RV and LV volume obtained from CT were inversely related with echocardiogrambased estimates of right ventricular systolic pressure using tricuspid regurgitation jet velocity (RVSP) and LV ejection fraction (LVEF) respectively. Patients with evidence of RV or LV dysfunction on echocardiogram had larger RV and LV dimensions on CT. Logistic regression models based on demographics and ventricular measures from CT had an area under the curve (AUC) of > 0.7 for the prediction of elevated RVSP and ventricular failure. These data suggest that non-cardiac gated, non-contrast enhanced thoracic CT scanning may provide insight into cardiac structure and function in smokers.

## Introduction

Cardiovascular disease is a major cause of morbidity in smokers and as much as 50% of the estimated 24 million patients in the US with chronic obstructive pulmonary disease (COPD) die of cardiovascular causes [1, 2]. While Echocardiography (ECHO) and cardiac magnetic resonance imaging (MRI) are often used to study cardiac structure and function in COPD[3], these are not routinely deployed in all smokers. Computed tomographic (CT) imaging of the chest is broadly utilized in clinical care and is increasingly used for lung cancer screening in high risk smokers[4]. Assessment of cardiac structure on those CT scans may help identify patients with COPD at greater risk for developing cardiac dysfunction. Rapid, non-invasive assessments of cardiac morphology and a better understanding of the functional interdependence of heart and lung may improve health care outcomes through early detection and initiation of treatment.

CT has been used to quantify coronary and thoracic aortic calcification [5], study the size of the pulmonary artery and aorta [2, 6–8] and described the relationship of parenchymal pulmonary vascular and disease progression[9, 10]. The caliber of other vessels such as the pulmonary veins has been explored as an image based metric of volume status [11].

Most screening CT scans and those obtained in large multi-center studies and trials are non-ecg gated and do not utilize contrast, posing significant limitation to cardiac segmentation and quantification of volume. While previous studies of manual measurements of RV/LV ratio have shown that ecg-gating is not strictly required for the specific markers of RV dilation in pulmonary embolus, these studies still utilized contrast[12]. Non-gated CT scans

lead to cardiac motion during the scan whereby the exact boundary of the heart depends on the cardiac cycle during which image is captured. Lack of contrast prevents simple segmentation of the ventricular septum.

Previously we developed a method to generate a surface model of the heart from ultrasound images[13, 14]. We sought to adapt this methodology to non-ecg gated and non-contrast thoracic CT scans and then explore the utility of the resulting data. We hypothesized that a model fit to the surface of the heart of non-cardiac gated volumetric CT data could provide assessments of ventricular size, shape, and function. To test this hypothesis we identified a subset of subjects enrolled in the COPDGene Study who underwent additional cardiac MRI or Echocardiographic assessments of the heart. While for the purpose of this study, the location of the heart was manually determined before deployment of cardiac fitting algorithm, fully automated algorithms may be developed that would then permit automated objective quantification of cardiac geometry from noncontrast non-ecg gated CT scans for further research and population screening purposes.

## Methods

### COPDGene Study

The COPDGene Study has been described in detail previously [15]. Briefly, it is a NHLBI funded investigation of the epidemiologic and genetic determinants of COPD in over 10,000 current and former smokers. Subjects with active lung diseases other than COPD and asthma were excluded from participation. Each subject underwent detailed characterization including spirometric assessments of lung function. Additional data collected included self reported physician diagnosed medical history. Volumetric CT scans of the chest were acquired at full inspiration following the standardized COPDGene Study imaging protocol with 120 kVp, tube current of 200 mAs, and 0.5 seconds rotation time. The COPDGene study was approved by the institutional review board at each participating clinical center, and all subjects provided written informed consent.

### Cardiac MRI Cohort

As part of the COPDGene study, 24 subjects free of a documented history of pulmonary vascular or cardiac disease additionally underwent cardiac MRI[16]. This cohort was used to validate the measurements of ventricular geometry against related measures made with MRI. Because this was a follow up study not part of the initial COPDGene recruitment, the MRI images were obtained about 3 years after the CT scan was obtained. Images were obtained using a 1.5 T scanner (Signa CV/i, GE Healthcare, Milwaukee, WI). A phased array cardiac coil, prospective electrocardiographic triggering and retrospective gating were utilized. Typical imaging parameters were field of view 36 to 44 cm, flip angle of 35 to 45 degrees, matrix size 256 in frequency domain and 128 to 256 in the phase domain, relaxation time of 3.7 to 4.1 ms, and Echocardiogramtime 1.5 to 1.7 msec. The end-diastolic (ED) horizontal long-axis image provided the reference from which a stack of contiguous short-axis slices of 8-mm thickness and 0-mm gap were obtained.

## Echocardiography Cohort

262 patients from a single center with clinically acquired Echocardiograms performed at the time of enrollment in COPDGene were retrospectively identified. These subjects underwent Echocardiographic assessment in addition to the standard evaluation performed at study enrollment. On average, these echocardiograms were obtained within 73 days of the CT Scan. Overall RV function, estimated right ventricular systolic pressure (RVSP), estimated left ventricular ejection fraction (LVEF), or comments about whether the LVEF was greater than or less than 55% were documented in subsets of the echocardiogram reports. This cohort was utilized to study the associations between ventricular geometry acquired from CT scan and both geometrical and functional correlates with echocardiography.

## Cardiac Modeling

A detailed overview of the methodology is provided in the supplement. Briefly, we used a statistical model of the human heart which uses 50 modes of variation (non-affine deformations of cardiac structure) to describe anatomic variability [17]. This model was developed from the anatomical segmentations of 3D+time data sets of 138 subjects including patients without disease as well as those with a broad range of pathologic conditions to facilitate generalization of the model.

The supervised segmentation process begins with a manual initialization of the average shape model within the region of interest (performed by trained operator) followed by an automated iteration of the deformation to optimize surface identification of the heart in the CT scan. The surface fitting is assisted by a "probabilistic driven initialization" to determine the boundary between pericardial fat and myocardium. This mode selected vertices in the normal direction of the manually initialized surface and examined the distribution of the attenuation values along those vertices in a window from −200 to 200 HU.

Based on the assumption that there are two tissues present in a single pathway (pericardial fat and then myocardium as one travels the path towards the centroid of the heart), a mixture of two components of non-central Gamma distributions was fitted in the attenuation window [18, 19]. The lower distribution in this window represented the pericardial fat while the higher attenuation distribution characterized the blood/muscle (Figure 2S). Voxels are then designated as belonging to either the fat or muscle and can be labeled as demonstrated in Figure 3S.

The metrics of cardiovascular morphology extracted included the free wall curvatures as well as estimates of the epicardial volume (wall + chamber). Endocardial volume (chamber size) for both the right and left ventricle were estimated based on atlas models of the heart that were fitted to the epicardial surface model. Herein these are referred to as the RV_EPI $\text{volume}_{CT}$, RV_ENDO $\text{volume}_{CT}$, LV_EPI $\text{volume}_{CT}$, and LV_ENDO $\text{volume}_{CT}$ respectively. All other measures of ventricular axes length and surface area, were obtained from the epicardial surface fitting model. Sphericity was defined as:

$$\text{Sphericity} = \pi^{\frac{1}{3}} \frac{(6V)^{\frac{2}{3}}}{S}$$

Where V is the volume and S is the surface area of the ventricle. The free wall was defined as the surface segments not in contact with the septum. The curvature estimate was defined as

$$\text{Curvature} = \sqrt{\frac{({k_1}^2 + {k_2}^2)}{2}}$$

Where $k_1$ is the minimum and $k_2$ is the maximum curvature of the surface[20].

### Statistical analysis

Data are presented as means and standard deviations or medians and interquartile ranges where appropriate. Intra-subject stability of measures were assessed with Pearson correlation coefficients. Concordance coefficients were used to assess intra and inter-operator agreement [21]. Associations between CT derived measures of cardiac morphology and MRI and ECHOCARDIOGRAMbased measures of cardiac structure and function were expressed using non-parametric (Spearman) correlation coefficients. Group to group comparisons were evaluated using the Wilcoxon rank sum test. Logistic Regression models [22] for outcomes of interest were created using a stepwise forward selection method using the measures of ventricular volume, as well as age at enrollment, gender, height and BMI. From these candidate variables, those with statistically significant p-values using Wald's test were retained in the model. Interaction terms were included in subsequent models if they reached statistical significance or if they exhibited a p value of less than 0.1 and improved model performance. Logistic regression models and ROC curve generation were performed using STATA 14 (StataCorp, College Station, Texas). All other statistical analyses were performed using SAS 9.3 (SAS institute, Cary, North Carolina). P values less than 0.05 were considered statistically significant.

## Results

### Reproducibility of CT based measures of ventricular geometry

Data from eleven subjects who had violated study protocol by enrolling at more than one center, and thus had received CT scans at both visits, were used to assess the intra-subject reproducibility. CT based measurements of all eleven subjects in the dual enrollment group (demographic information shown in Table 1, **Column A**) was performed by a single operator. The second CT scan in the dual enrollment cohort occurred at a median interval of 201 days from the first scan. There was a strong correlation between the first and second baseline measures of RV and LV volume (R=0.86, P<0.001; R=0.87, P<0.001 respectively).

The MRI cohort was used to explore the intra- and inter-operator reproducibility in fitting the heart surface model to the CT scan. The demographics for the MRI cohort is shown in Table 1, **Column B**. The mean age for this cohort was 59±9 years with a mean FEV1 of 52±16 percent of predicted. Intra-operator agreement on assessments of RV and LV volume was excellent with concordance coefficients 0.92 and 0.98 for RV and LV volume, respectively (Table S1). Inter-concordance coefficients shown in Table S-2, with concordance coefficients ranging from 0.91 to 0.97.

### Validation of CT based ventricular geometry as compared to MRI measures

The associations of CT and MRI assessments of ventricular dimensions were explored using data from MRI cohort and is presented in Table 2. The CT based estimates of RV volume (RV_EPI $volume_{CT}$ and RV_ENDO $volume_{CT}$) were significantly associated with both the end diastolic RV volume (RV ED $volume_{MR}$) and Mass (RV ED $mass_{MR}$) obtained from MRI. There were similarly significant associations between CT and MRI left ventricular measures. Computed tomographic based estimates of the long axis dimension of the LV (LV Long $Axis_{CT}$) were related to this same measure (LV ED $length_{MR}$) obtained from MR as were measures of the free wall curvature of the ventricle (LV Free Wall $curvature_{CT}$ and LV mid ED $curvature_{MR}$). The sphericity of the LV on CT scan (LV $sphericity_{CT}$) was also significantly related to the long to short axis radius ratio of the LV obtained from MRI (LV ED radius $ratio_{MR}$). Finally, the CT derived ratio of RV to LV volume (RV/LV volume $ratio_{CT}$) was significantly associated with the ratio of those same measures obtained from MRI (RV/LV ED volume $ratio_{MR}$).

### Association between CT based ventricular geometry and cchocardiographic based ventricular structure and function

Examples of chamber models reconstructed for three subjects with echocardiograms are shown in Figure 1. The mean age for the echocardiogram cohort was 64.7±9 years with a mean FEV1 of 47±23 percent predicted (Additional demographic information in Table 1, **column C**). The RV Long $Axis_{CT}$ and the RV short $Axis_{CT}$ were significantly associated with RV Minor $axis_{ECHO}$ obtained from Echo. The RV_EPI and RV_ENDO $volume_{CT}$ and RV surface $area_{CT}$ were also related to Echocardiogramderived axis measurements. One hundred and ninety four of the 262 Echocardiograms reported an estimated RV systolic pressure (RVSP). This RVSP was directly related to CT measures of RV size (RV_EPI $volume_{CT}$, RV_ENDO $volume_{CT}$, RV Long $Axis_{CT}$, RV Short $Axis_{CT}$, RV surface $area_{CT}$). In addition, 130 of the Echocardiogramreports were noted to have descriptions of RV function as being normal (n=120) or decreased (n=10). There were statistically significant differences in the CT based measures of RV size in those with decreased RV function versus those with preserved function (Table 3).

A subset of the Echocardiogramreports also provided an additional qualitative description of LV function (n=180 where the LV function was categorized as “normal” or “reduced”) while some had quantitative estimates of the LV ejection fraction (LV EF; n=98 subjects). There were statistically significant differences in the CT estimates of LV size and morphology between subjects with reduced LV function (N = 18) and those with normal LV function (N = 162) (Table 4). Subjects with a reduced Ejection Fraction (EF) had larger LV size with lesser free wall curvature on CT scan. In the subjects with quantitative measurement of LV ejection fraction, a larger LV size and reduced free wall curvature were also predictive of reduced LVEF.

Logistic regression models were constructed for the following variables: elevated RVSP (RVSP > 40mmHg), reduced RV function and reduced LV EF (Table 5). RV volume was a statistically significant predictor of both RVSP and RV Failure, with gender and age being independent predictors and effect modifiers of this association. The final model for RVSP

which included RV volume, age, gender and the interaction terms, had an AUC of 0.77. The final model for RV failure included age and gender and had an AUC of 0.76. Left ventricular volume (LV_EPI $volume_{CT}$) was predictive of decreased LV ejection fraction and with the addition of BMI the final model with had an AUC of 0.71.

## Discussion

Computed tomographic characterization of thoracic disease in smokers is increasingly leveraged for clinical, epidemiologic, and genetic investigation. While previous investigations have demonstrated the utility of CT based assessments of the vascular tree and atherosclerosis in smokers, little literature exists on directly modeling the heart from non-ecg-gated, non-contrast CT data. Herein we report the development and application of a model of cardiac structure based upon a surface fitting algorithm applied to non-cardiac gated, non- contrast enhanced images. From this initial fit of the epicardial surface we made inferences about the right and left epicardial (wall and chamber) as well as endocardial (chamber) ventricular size and shape. We found that CT based measures of right and left ventricular shape and size were significantly associated with MRI and Echocardiogrambased assessments of these same chambers. We further found that such CT based morphology had discriminatory power in detecting abnormal ventricular function detected by Echocardiography.

Magnetic resonance imaging is considered a gold standard for the non-invasive assessment of the cardiac structure. It can provide detailed assessments of ventricular morphology and function without decrements in image quality that are observed using Echocardiography in hyper-inflated patients with COPD. Using data from 24 subjects who underwent CT and MRI we found highly statistically significant associations between CT and MR based measures of ventricular size and morphology. Up to 50% of the variance in the MRI based measures of ventricular structure were explained by the CT data. These associations were strongest with CT based measures of LV free wall curvature and tended to weaken with measures of volume. The latter is not surprising since the CT based model relies on statistical inference of septal location and morphology. Because the cardiac MRI studies were obtained three years after the CT data, changes in the cardiovascular state of the subjects in the interim could also introduce a difference between the two measurements.

There were also significant associations between our CT measures of ventricular morphology and similar assessments obtained from Echocardiography. These correlations were of the same direction and magnitude as those observed in the MRI data. The larger sample size of echocardiogram data allowed additional exploration of CT structure and cardiac function. In this data we again found highly plausible associations. Subjects with larger RVs on CT were more likely to have elevated pulmonary arterial pressures (RVSP) and decreased RV function. Subjects with an enlarged left ventricle and reduced curvature of the free wall on CT scan tended to have lower estimated LV ejection fractions on echocardiogram. These findings were further corroborated in regression models adjusted for subject age and sex where the areas under the curve (AUC) were greater than 0.75 (Figure 2). We suspect that the reasons for this are not found in the detection of cardiac displacement on CT but rather the relationship of chamber structure and function. Deviations in structure

likely connote deviations in function where for example an enlarged left ventricle is less likely to exhibit a normal ejection fraction.

There are several limitations to this work that must be acknowledged. The first is the nature of the data obtained from the CT based surface fitting model. Since the cardiac structures below the epicardial surface are indiscernible on non-contrast enhanced, non cardiac gated CT scans, metrics of RV and LV size were highly dependent upon accurate estimates of the location of the inter-ventricular septum. This is likely why the strongest correlations between CT and MR tended to be those assessing surface morphology rather than volume. CT scans were obtained with an inspiratory hold whereas measurements in cardiac MRI are often obtained during expiratory breath holds. The type of breath hold used in cardiac MRI and echocardiography can significantly alter diaphragm position and preload thus altering measurements of chamber geometry. It must also be noted that the measures of curvature from the MRI were obtained from the cardiac MRI report and were not replicated using our techniques. It is highly likely that there are differences in the location and technique used to assess free wall curvature between the CT and MRI data. Subtle differences in such techniques may result in large differences in estimates given the eccentric surface of the ventricles. The association of CT and MRI based measures of ventricular morphology would likely be further improved if the same operator performed the assessments using a single technique. Another limitation to this investigation is the number of subjects and timing of the MRI data collection, which was obtained 3 years after the CT scan. While this likely introduced a source of error in the comparison between cardiac MRI and CT scan, there is no a priori reason to suspect that this would lead to overestimating the agreement between the two modalities while it is likely that it may have accounted for part of the discrepancy between the two measurements. The small sample size prevented detailed examination of CT morphology and MRI measures of cardiac function. Progression of disease and changes in volume status between the two imaging time-points complicated this comparison.

In conclusion, estimates of right and left ventricular size and morphology can be obtained from volumetric CT data. These measures are associated with structural and functional data obtained from MRI and Echocardiographic techniques. These techniques have the capability of becoming fully automated and incorporated into the clinical reporting of CT data. Significant numbers of CT scans are obtained in patients with lung disease, dyspnea, and smokers, all of whom are at risk for cardiovascular disease and in the appropriate clinical settings, findings of abnormal cardiac geometry on CT scan would then warrant further cardiac examination. Cohorts specifically designed for assessing the performance of these methods in screening for cardiovascular disease are necessary to validate this method and to optimize to minimize unnecessary follow-up testing while improving clinical value. Additionally, methods of automated quantification of cardiac geometry can be broadly deployed in CT based clinical, epidemiologic, and genetic investigation of diseases affecting the chest.

## Supplementary Material

Refer to Web version on PubMed Central for supplementary material.

## Acknowledgments

Authors in this study were supported by Supported by NHLBI grants 5T32HL007633 (FNR), 1R01HL116931 (R.S.J.E. and G.R.W). K08 HL123940 (JMW).

## References

1. Divo M, Cote C, de Torres JP, Casanova C, Marin JM, Pinto-Plata V, Zulueta J, Cabrera C, Zagaceta J, Hunninghake G, Celli B. Comorbidities and risk of mortality in patients with chronic obstructive pulmonary disease. American journal of respiratory and critical care medicine. 2012; 186:155–61. [PubMed: 22561964]
2. Sin DD, Man SF. Chronic obstructive pulmonary disease as a risk factor for cardiovascular morbidity and mortality. Proceedings of the American Thoracic Society. 2005; 2:8–11. [PubMed: 16113462]
3. Rahaghi FN, van Beek EJ, Washko GR. Cardiopulmonary coupling in chronic obstructive pulmonary disease: the role of imaging. Journal of thoracic imaging. 2014; 29:80–91. [PubMed: 24552883]
4. Eberth JM. Lung Cancer Screening With Low-Dose CT in the United States. Journal of the American College of Radiology : JACR. 2015; 12:1395–402. [PubMed: 26614885]
5. Budoff MJ, Nasir K, Kinney GL, Hokanson JE, Barr RG, Steiner R, Nath H, Lopez-Garcia C, Black-Shinn J, Casaburi R. Coronary artery and thoracic calcium on noncontrast thoracic CT scans: comparison of ungated and gated examinations in patients from the COPD Gene cohort. Journal of cardiovascular computed tomography. 2011; 5:113–8. [PubMed: 21167806]
6. Wells JM, Washko GR, Han MK, Abbas N, Nath H, Mamary AJ, Regan E, Bailey WC, Martinez FJ, Westfall E, Beaty TH, Curran-Everett D, Curtis JL, Hokanson JE, Lynch DA, Make BJ, Crapo JD, Silverman EK, Bowler RP, Dransfield MT. Pulmonary arterial enlargement and acute exacerbations of COPD. The New England journal of medicine. 2012; 367:913–21. [PubMed: 22938715]
7. Ng CS, Wells AU, Padley SP. A CT sign of chronic pulmonary arterial hypertension: the ratio of main pulmonary artery to aortic diameter. Journal of thoracic imaging. 1999; 14:270–8. [PubMed: 10524808]
8. Kurugol S, Come CE, Diaz AA, Ross JC, Kinney GL, Black-Shinn JL, Hokanson JE, Budoff MJ, Washko GR, San Jose Estepar R. Automated quantitative 3D analysis of aorta size, morphology, and mural calcification distributions. Medical physics. 2015; 42:5467–78. [PubMed: 26328995]
9. Matsuoka S, Washko GR, Yamashiro T, Estepar RS, Diaz A, Silverman EK, Hoffman E, Fessler HE, Criner GJ, Marchetti N, Scharf SM, Martinez FJ, Reilly JJ, Hatabu H, National Emphysema Treatment Trial Research G. Pulmonary hypertension and computed tomography measurement of small pulmonary vessels in severe emphysema. American journal of respiratory and critical care medicine. 2010; 181:218–25. [PubMed: 19875683]
10. Estepar RS, Kinney GL, Black-Shinn JL, Bowler RP, Kindlmann GL, Ross JC, Kikinis R, Han MK, Come CE, Diaz AA, Cho MH, Hersh CP, Schroeder JD, Reilly JJ, Lynch DA, Crapo JD, Wells JM, Dransfield MT, Hokanson JE, Washko GR, Study CO. Computed tomographic measures of pulmonary vascular morphology in smokers and their clinical implications. American journal of respiratory and critical care medicine. 2013; 188:231–9. [PubMed: 23656466]
11. Smith BM, Prince MR, Hoffman EA, Bluemke DA, Liu CY, Rabinowitz D, Hueper K, Parikh MA, Gomes AS, Michos ED, Lima JA, Barr RG. Impaired left ventricular filling in COPD and emphysema: is it the heart or the lungs? The Multi-Ethnic Study of Atherosclerosis COPD Study. Chest. 2013; 144:1143–51. [PubMed: 23764937]
12. Lu MT, Cai T, Ersoy H, Whitmore AG, Levit NA, Goldhaber SZ, Rybicki FJ. Comparison of ECG-gated versus non-gated CT ventricular measurements in thirty patients with acute pulmonary embolism. Int J Cardiovasc Imaging. 2009; 25:101–7. [PubMed: 18626787]
13. Haak A, Ren B, Mulder HW, Vegas-Sanchez-Ferrero G, van Burken G, van der Steen AF, van Stralen M, Pluim JP, van Walsum T, Bosch JG. Improved Segmentation of Multiple Cavities of the Heart in Wide-View 3-D Transesophageal Echocardiograms. Ultrasound in medicine & biology. 2015; 41:1991–2000. [PubMed: 25864017]

14. Haak AM, H W, Ren B, Vegas-Sanchez-Ferrero G, van Burken G, van der Steen AFW, van Stralen M, Pluim JPW, van Walsum T, Bosch JG. Segmentation of multiple heart cavities in wide-view fused 3D transesophageal echocardiograms. Ultrasonics Symposium (IUS), 2014 IEEE International. 2014:691–694.
15. Regan EA, Hokanson JE, Murphy JR, Make B, Lynch DA, Beaty TH, Curran-Everett D, Silverman EK, Crapo JD. Genetic epidemiology of COPD (COPDGene) study design. Copd. 2010; 7:32–43. [PubMed: 20214461]
16. Wells JM, Iyer AS, Rahaghi FN, Bhatt SP, Gupta H, Denney TS, Lloyd SG, Dell'Italia LJ, Nath H, Estepar RS, Washko GR, Dransfield MT. Pulmonary artery enlargement is associated with right ventricular dysfunction and loss of blood volume in small pulmonary vessels in chronic obstructive pulmonary disease. Circulation Cardiovascular imaging. 2015; 8
17. Hoogendoorn C, Duchateau N, Sanchez-Quintana D, Whitmarsh T, Sukno FM, De Craene M, Lekadir K, Frangi AF. A high-resolution atlas and statistical model of the human heart from multislice CT. IEEE transactions on medical imaging. 2013; 32:28–44. [PubMed: 23204277]
18. Vegas-Sanchez-Ferrero G, Aja-Fernandez S, Palencia C, Martin-Fernandez M. A generalized gamma mixture model for ultrasonic tissue characterization. Computational and mathematical methods in medicine. 2012; 2012:481923. [PubMed: 23424602]
19. Vegas-Sanchez-Ferrero G, Seabra J, Rodriguez-Leor O, Serrano-Vida A, Aja-Fernandez S, Palencia C, Martin-Fernandez M, Sanches J. Gamma mixture classifier for plaque detection in intravascular ultrasonic images. IEEE transactions on ultrasonics, ferroelectrics, and frequency control. 2014; 61:44–61.
20. Koenderink JJ, van Doorn AJ. Surface shape and curvature scales. Image and vision computing. 1992; 10:557–564.
21. Lin LI. A concordance correlation coefficient to evaluate reproducibility. Biometrics. 1989; 45:255–68. [PubMed: 2720055]
22. Hosmer, DW., Lemeshow, S., Sturdivant, RX. Applied logistic regression. Third. New Jersey: John Wiley & Sons, Inc.; 2013.

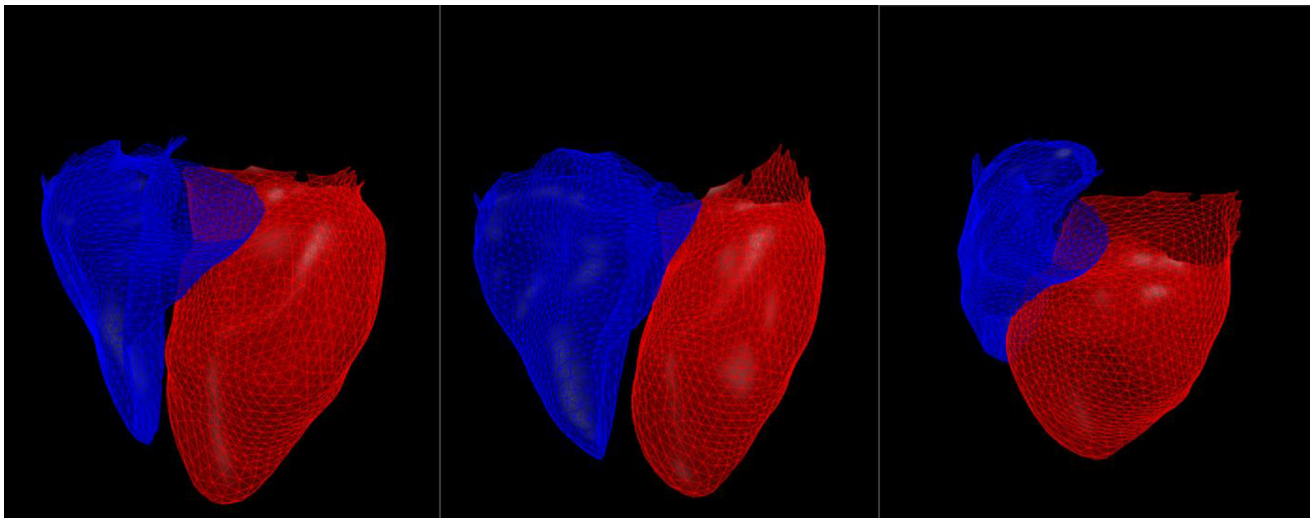

**Figure 1.**

The right ventricle (blue) and left ventricle (red) in three subjects with a cardiac model fitted to the surface of the heart using volumetric non-contrast CT scan. A subject with Gold 0 disease and with an RV/LV ratio of 0.5, RVSP of 20 and no evidence of ventricular dysfunction (A), A subject with Gold 3 disease an RV/LV ratio of 0.8, RV dilation, elevated RVSP of 47 (B), and a subject with Gold 2 disease with LV dilation and ejection fraction of 35%.

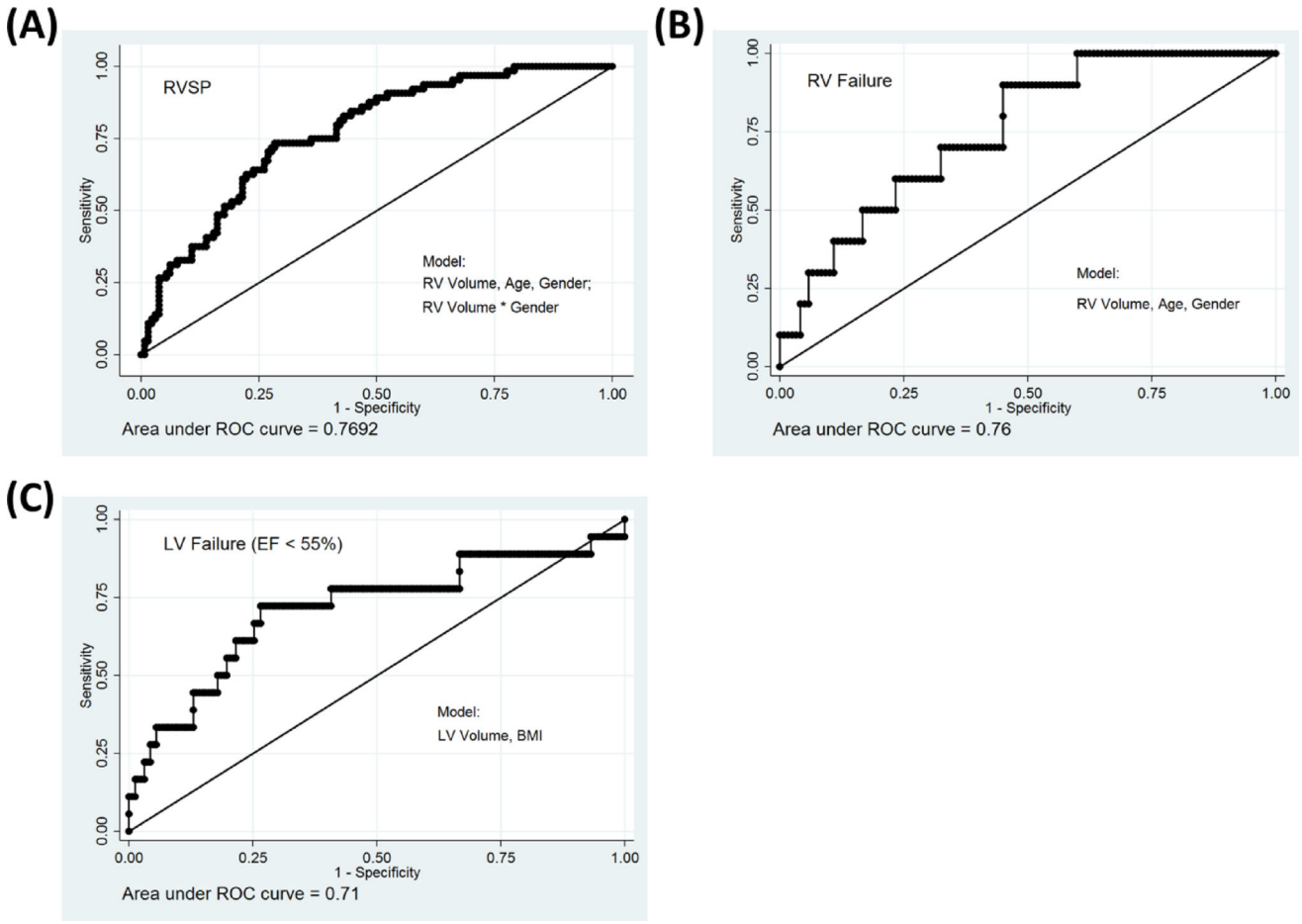


**Figure 2.**

Model Discrimination Performance as measured by the Area under the ROC, shown for four logistic regression models constructed using a stepwise forward selection method for markers of cardiac dysfunction in the cohort with available Echocardiograms. A model of ability to predict RVSP ≥ 40 (A), RV failure as marked on the Echocardiogram (B), LV failure defined by EF < 55% (C).

## Table 1

Demographics of two cohorts used in this study, both subsets of the COPDGene Study. Data represent as n (%) and mean (±SD).

| Variable | (A) Dual Enrollment (N = 11) | (B) MRI Cohort (N = 24) | (C) Echo Cohort (N = 262) |
|---|---|---|---|
| **Demographics** | | | |
| Age (Years) | 52±8 | 59±9 | 65±9 |
| White Race | 10 (91%) | 14 (58%) | 250 (95%) |
| Male Sex | 11 (100%) | 16 (67%) | 126 (48%) |
| BMI | 29±9 | 29±8 | 28±7 |
| BSA ($m^2$) | 2.06±0.25 | 1.99±0.22 | 1.93±.28 |
| 6 Minute Walk Distance (ft) | 1105±552 | 1069±209 | 1173±365 |
| **Lung Function** | | | |
| $FEV_1$ % predicted | 70±22 | 57±27 | 47±23 |
| $FEV_1$:FVC Ratio | 0.68±0.17 | 0.52±0.16 | 0.46±0.17 |
| TLCpp (Race Adjusted, L) | 76±20 | 102±14 | 106±19 (N = 257) |
| **MRI** | | | |
| LVEF (%) | | 64±8 | |
| RVEF (%) | | 58±10 | |
| RVESVI | | 24±9 | |
| RVMI | | 13±4 | |
| **ECHO** | | | |
| RV Minor Axis | | | 3.24±0.54 (N = 238) |
| RVSP | | | 36.0±13.22 |
| LVEF (%) | | | 64.1±7.7 |

BMI, body mass index; BSA, estimated body surface area; $FEV_1$, forced expiratory volume in 1 second; FVC, forced vital capacity. TLCpp, Total Lung Capacity, percent predicted; LVEF, left ventricular ejection fraction; RVEF, right ventricular ejection fraction; RVESVI, right ventricular end systolic volume index; RVMI, right ventricular mass index; PA/A ratio, the ratio of the PA diameter to aortic diameter.

## Table 2

Correlation coefficient (R) between CT derived cardiac volume measurements and cardiac MRI based volume and mass estimates in 24 subjects.

| | **Cardiac MRI Derived Metrics** | |
|---|---|---|
| **CT Derived Metrics** | **RV ED Volume$_{MR}$** | **RV ED Mass$_{MR}$** |
| **RV_EPI Volume$_{CT}$** | 0.65 (0.0006) | 0.60 (0.002) |
| **RV_ENDO Volume$_{CT}$** | 0.61 (0.001) | 0.57 (0.004) |
| | **LV ED volume$_{MR}$** | **LV ED mass$_{MR}$** |
| **LV_EPI volume$_{CT}$** | 0.61 (0.001) | 0.56 (0.004) |
| **LV_ENDO volume$_{CT}$** | 0.60 (0.002) | 0.51(0.01) |
| | **LV ED length$_{MR}$** | |
| **LV Long Axis$_{CT}$** | 0.49 (0.02) | |
| | **LV mid ED curvature$_{MR}$** | |
| **LV Free Wall curvature$_{CT}$** | 0.70 (0.0001) | |
| | **LV ED radius ratio$_{MR}$** | |
| **LV sphericity$_{CT}$** | 0.51 (0.01) | |
| | **RV/LV ED volume ratio$_{MR}$** | |
| **RV/LV volume ratio$_{CT}$** | 0.46 (0.02) | |

ED = end diastolic; LV = left ventricular; RV = right ventricular; MID = middle of ventricle. Spearman correlation coefficients, with accompanying p-values.

**Table 3**

Correlation of CT derived right ventricular geometry with echocardiogram derived geometric and functional measures (first three columns) and the difference in those metrics between patients characterized has having abnormal versus normal RV function.

| | Echocardiogram Derived Measures | | | | |
|---|---|---|---|---|---|
| **CT Derived Measures of Right Ventricle** | **RV Minor axis$_{ECHO}$ (N = 238)** | **RVSP (N = 194)** | **Decreased RV Function (N = 10 )** | **Normal RV function (N = 120)** | **p** |
| RV Long Axis$_{CT}$ | R = 0.36, p < 0.0001 | R = 0.28, p < 0.0001 | 7.3[6.1–7.5] | 6.9[6.4–7.3] | 0.44 |
| RV short Axis$_{CT}$ | R = 0.44, p < 0.0001 | R = 0.27, p = 0.0002 | 4.3[4.0–4.7] | 4.0[3.6–4.3] | 0.03 |
| RV_EPI volume$_{CT}$ | R = 0.46, p < 0.0001 | R = 0.3, p < 0.0001 | 106[87–117] | 85[66–103] | 0.04 |
| RV_ENDO volume$_{CT}$ | R = 0.45 P < 0.0001 | R = 0.28 P = 0.0001 | 67[54–79] | 57[42–67] | 0.06 |
| RV surface area$_{CT}$ | R = 0.49, p < 0.0001 | R = 0.24, p = 0.0006 | 169[142–194] | 148[130–169] | 0.05 |

RV = right ventricle; RA = right atrium; RVSP = estimated right ventricular systolic pressure by echocardiogram. Values shown are spearman correlation coefficients (R) and p-values associated with spearman correlation. Values shown for subgroups with decreased and normal RV function are shown as median [interquartile range].

## Table 4

Correlation of CT derived left ventricular geometry with echocardiogram derived functional measures (first three columns) and the difference in those metrics between patients characterized has having abnormal versus normal left ventricular ejection fraction.

| | ECHO Derived Measures | | | |
|---|---|---|---|---|
| **CT Measures of Left Ventricle** | **LVEF (N = 98)** | **Reduced EF (N = 18)** | **Normal EF (N = 162)** | **P value** |
| LV Long $Axis_{CT}$ | R = −0.20, p = 0.05 | 8.54[7.69–9.21] | 8.05[7.42–8.62] | 0.08 |
| LV_EPI $volume_{CT}$ | R = −0.22, p = 0.03 | 207.1[167.5–240.1] | 173.1[143.8–199.2] | 0.01 |
| LV_ENDO $volume_{CT}$ | R = −0.23, p = 0.03 | 118.0[89.0–141.1] | 97.1[78.4–111.6] | 0.02 |
| LV $surface\ area_{CT}$ | R = −0.21, p = 0.03 | 202.7[164.1–223.7] | 176.6[153.1–197.0] | 0.03 |
| LV $Volume/Surface\ Area_{CT}$ | R = −0.18, p = 0.08 | 1.03[0.98–1.07] | 0.97[0.92–1.02] | 0.009 |
| LV Free Wall $Curvature_{CT}$ | R = 0.20, p = 0.04 | 0.018 [0.0169–0.0195] | 0.0192[0.18–0.0205] | 0.03 |

LV = left ventricle; EF = ejection fraction;. Values shown are correlation coefficients (R) and p-values associated with spearman correlation. Values shown for subgroups with decreased and normal ejection fraction are shown as median [interquartile range].

## Table 5

Logistic regression model performance based on AUC (Area Under The Curve) for models predicting RVSP > 40, reduced RV function, reduced LV ejection fraction and history of CHF.

| | RVSP > 40 N = 194 (64 /194) | Reduced RVF N = 130 (10/130) | Reduced LVEF N = 180 (18/180) | |
|---|---|---|---|---|
| **Model Variables** | **AUC** | **AUC** | **Model Variables** | **AUC** |
| **RVV** | 0.67 | 0.70 | **LVV** | 0.68 |
| **RVV**<br>**Age**<br>**Gender** | 0.75 | 0.75 | **LVV**<br>**BMI** | 0.71 |
| **RVV**<br>**Age**<br>**Gender**<br>**RVV*Gender** | 0.77 | | | |

RV = Right Ventricle; LV = Left Ventricle. RVV = Right Ventricle Volume. LVV = Left Ventricle Volume. TVV = Total Ventricular Volume, a sum of RVV and LVV. FWC = LV free wall curvature. RVSP = estimated right ventricular systolic pressures by echocardiogram. RVF = evidence of RV failure on echocardiogram; LVEF = left ventricular ejection fraction. CHF = subject reported diagnosis of congestive heart failure.